Quantifying Mangrove Forest Attributes Using Terrestrial Laser Scanning

Dunlop, Thomas; Mancheño, Alejandra Gijón; Glamore, William; Felder, Stefan; van Wesenbeeck, Bregje K.

DOI
10.1007/s12237-025-01533-0

Publication date
2025

Document Version
Final published version

Published in
Estuaries and Coasts

Citation (APA)
Dunlop, T., Mancheño, A. G., Glamore, W., Felder, S., & van Wesenbeeck, B. K. (2025). Quantifying Mangrove Forest Attributes Using Terrestrial Laser Scanning. *Estuaries and Coasts*, *48*(4), Article 108. https://doi.org/10.1007/s12237-025-01533-0

Estuaries and Coasts (2025) 48:108
https://doi.org/10.1007/s12237-025-01533-0

Quantifying Mangrove Forest Attributes Using Terrestrial Laser Scanning

Thomas Dunlop[1,2] · **Alejandra Gijón Mancheño**[2] · **William Glamore**[1] · **Stefan Felder**[1] · **Bregje K. van Wesenbeeck**[2,3]

Received: 8 January 2025 / Revised: 20 March 2025 / Accepted: 31 March 2025

Abstract

Mangroves are increasingly recognised for their ecosystem services, including their capacity to store carbon and adapt to climate pressures by stabilising shorelines and acting as storm barriers. To quantify these services, relevant parameters such as mangrove biomass and drag coefficients have been calculated using allometric equations fitted to field measurements of physical mangrove attributes. However, previous research to quantify mangrove attributes has involved time-consuming hand measurements and long processing times associated with terrestrial laser scanning (TLS). To more efficiently capture and process mangrove attributes, such as the density, diameter, height, and projected area of stems and roots, a novel method for collecting mangrove field data using TLS was developed. Recorded TLS data were compared to field measurements conducted in 12 *Avicennia marina* forests across 10 estuaries and 4 unique estuary typologies. The results demonstrated the reliable estimation of mangrove attributes using TLS and revealed a link between these attributes and estuarine geomorphology. Mangrove stems were accurately identified in all estuary typologies, with attribute estimations more accurate for forests in Drowned River Valleys (DRVs). A sensitivity analysis revealed that 10–20 trees for DRVs and 35–45 trees for barrier estuaries require point cloud processing to characterise a forest area of 400–1300 m^2 and to achieve convergent stem diameter and tree height results. The method presented herein offers an efficient way to quantify aboveground stem and root attributes and the surface area of mangrove trees. This data can be used to characterise mangrove forests worldwide and provide fundamental attributes for quantifying ecosystem services.

Keywords Allometry · *Avicennia marina* · Mangrove · Point cloud · Projected area · Terrestrial laser scanning (TLS)

Introduction

Mangrove forests are increasingly recognised for the range of ecosystem services they provide, including recreation and ecotourism (Reid, 2005), fisheries support (Faunce & Serafy, 2006), and habitat provision (Miedema Brown & Anand, 2022). In addition, the capacity of mangroves to sequester and store carbon in their roots, soil, and aboveground biomass has motivated mangrove restoration projects to mitigate greenhouse gas emissions (Alongi, 2014). Mangroves can also aid adaptation to climate change effects by trapping sediment and raising bed levels (Lovelock et al., 2011), reducing hydrodynamic forces of storm surges (Menéndez et al., 2020), and dampening waves (van Zelst et al., 2021).

Mangrove forest characteristics, such as health, density, and size, influence the value and magnitude of provided ecosystem services (Miedema Brown & Anand, 2022). For example, blue carbon stocks (Sippo et al., 2020) are usually calculated using allometric relationships for aboveground biomass (AGB) and belowground biomass (BGB) (Komiyama et al., 2008), which depend on the trunk diameter at breast height (DBH) (Komiyama et al., 2008) and tree height (Chave et al., 2005; Komiyama et al., 2005), but often neglect aboveground root systems (Feliciano et al., 2014).

Communicated by Paul A. Montagna

✉ Thomas Dunlop
t.dunlop@unsw.edu.au

[1] Water Research Laboratory, School of Civil and Environmental Engineering, UNSW Sydney, 110 King St, Manly Vale, NSW 2093, Australia

[2] Department of Hydraulic Engineering, Delft University of Technology, Delft, GA 2600, The Netherlands

[3] Unit for Marine and Coastal Systems, Deltares, Delft, MH 2600, The Netherlands

Published online: 30 April 2025

Allometric relationships between mangrove properties may similarly be derived for coastal protection services (Twomey & Lovelock, 2025). Drag coefficients (Horstman et al., 2021; Mazda et al., 1997), damping coefficients (Lopez-Arias et al., 2024; Maza et al., 2021; Zhang et al., 2023), roughness values (Zhang et al., 2012), and projected surface areas (Zhang et al., 2023) are all influenced by the submerged portion of stems and roots. Many studies have quantified drag and damping coefficients using simplified profiles of mangroves for ease of construction and computational efficiency (Menéndez et al., 2020; Suzuki et al., 2012; van Zelst et al., 2021), with the vertical profile being divided into three layers of canopy, stem, and roots, where the stems and roots are represented by vertical cylinders (Suzuki et al., 2012). However, these three-layer profiles have not been validated with surface area measurements from the field.

To better define mangrove characteristics, additional field measurements in diverse forests are needed. To date, remote sensing techniques, such satellite imagery and airborne laser scanning with unmanned aerial vehicles (UAVs), have been used to map mangrove extent (Bunting et al., 2018; Giri et al., 2011), canopy height (Navarro et al., 2020; Simard et al., 2025), and canopy diameter (Navarro et al., 2020) but have faced difficulty capturing understory features at an individual tree level (Hyyppä et al., 2020). In the field, most datasets of mangrove understory attributes have been collected by hand and without remote sensing equipment. Ground-based LiDAR technologies, such as iPhone LiDAR (Luetzenburg et al., 2024), handheld laser scanning, backpack laser scanning, and under-canopy UAVs (Hyyppä et al., 2020), have been used to efficiently measure tree stems with diameters greater than 10 cm, but with larger errors for stems less than 10 cm (Ryding et al., 2015). This may be due to the ranging accuracies of handheld and UAV scanning devices, which are in the order of centimetres (Hyyppä et al., 2020). This accuracy limits the effective measurements of thin mangrove stems and root systems. To capture data with millimetre accuracy, terrestrial laser scanning (TLS) has been used, particularly to map space-time variations in topography and built structures (Wu et al., 2022), but with longer scan and setup times than handheld devices (Ryding et al., 2015).

TLS has also been successfully applied in forestry since the early 2000s (Calders et al., 2020), with greater success detecting and measuring the stem diameter of individual trees in low density terrestrial forests with minimal occlusion and shrub presence (Zhao et al., 2023). However, TLS has rarely been utilised to quantify mangrove properties. Existing research with TLS in mangrove forests has targeted a few sites with multiple mangrove species, including *Rhizophora apiculata*, *Xylocarpus granatum*, *Sonneratia alba*, *Bruguiera gymnorrhiza* (Kargar et al., 2020), *Rhizophora mangle*, *Laguncularia racemosa* (Feliciano et al., 2014), *Avicennia germinans* (Feliciano et al., 2014; Olagoke et al., 2016), *Aegiceras corniculatum*, and *Avicennia marina* (Warfield & Leon, 2019), with one study applying TLS across five *Avicennia marina* sites (Owers et al., 2018). These studies have reliably calculated DBH with a TLS device to an accuracy of 74% of field measurements (Kargar et al., 2020) and have accurately classified stems based on manual inspection of point clouds (Kargar et al., 2020). Past research has also calculated individual mangrove biomass, volume, and specific wood densities using TLS (Feliciano et al., 2014; Kargar et al., 2020; Olagoke et al., 2016; Owers et al., 2018). Total forest volume was also captured in detail, with effective data capture below the canopy in areas with limited occlusion (Warfield & Leon, 2019). These studies involved co-registering multiple scans and manually separating mangrove stems from branches, canopies, and roots. This was undertaken by either pre-training a dataset for classification (Kargar et al., 2020) or manually removing background vegetation, with processing times between 1 and 12 hours for each individual tree (Olagoke et al., 2016). While these studies have investigated the physical attributes of mangrove stem diameter and volume in a few forests, substantial data and knowledge gaps remain associated with the use of TLS to process point cloud data across different environments to quantify the density, diameter, height, and projected area of stems and roots, without the need to co-register scans nor manually classify mangrove attributes.

In this study, a systematic method applicable across mangrove genera has been developed for capturing and processing the physical attributes and projected areas of *Avicennia marina* mangrove forests at 12 sites across 4 different estuary typologies. This novel method utilises TLS and a desktop-based analysis with CloudCompare (2023) and Python to quantify mangrove characteristics. Single forest scans are processed without co-registration of scans nor manual pre-training of datasets for attribute classification. The method presented herein outlines a step-by-step process that practitioners can follow to conduct efficient field surveys of mangrove forests and to process the results for the quantification of physical mangrove attributes.

Materials and Methods

Study Area

The mangrove forests selected for this study spanned 12 sites across 10 estuaries in southeastern Australia (Fig. 1a). To test the applicability of the method to different environmental settings, the estuaries covered four typologies based on the following characteristics:

1) Drowned River Valley (DRV), characterised by a deep entrance and tidal amplification from the ocean to the upper reaches of the estuary (Hanslow et al., 2018).

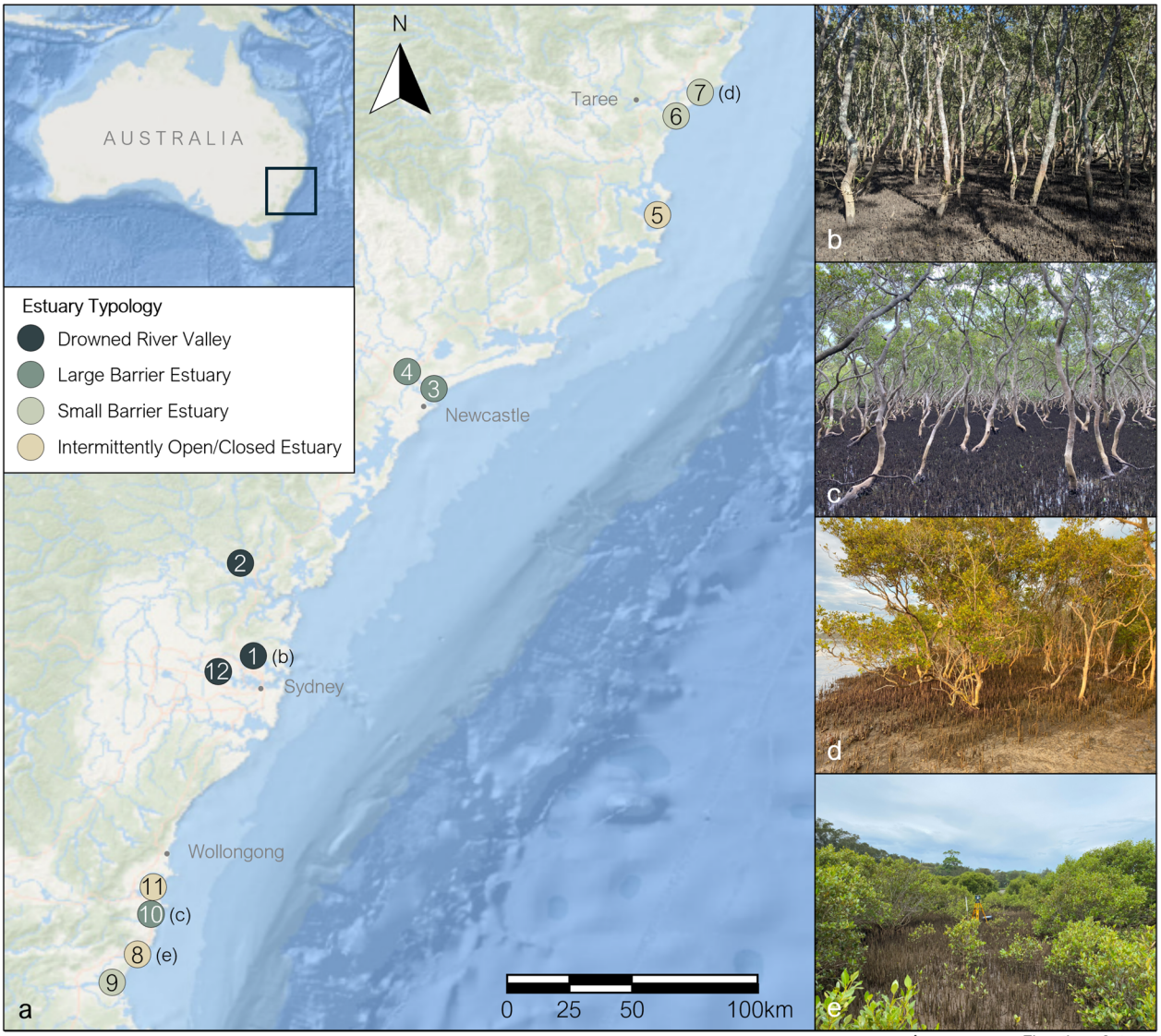

Site	Estuary typology	Date of visit	Mean tidal range[1] (m)	Cross-shore forest width[2] (m)	No. of scans	Average distance between scans (m)	Elevation of stem diameter measurement (m)
1. Middle Harbour South	DRV	06.12.23	0.993	150	3	29	1.37
2. Spencer, Hawkesbury River	DRV	12.12.23	1.095	250	3	34	1.37
3. Stockton Sandspit, Hunter River	LBE	12.12.23	1.036	30	4	31	1.37
4. Kooragang Island, Hunter River	LBE	12.12.23	0.978	45	2	40	1.37
5. Tiona, Wallis Lake	IOCE	13.12.23	0.135	15	3	22	1.37
6. Oyster Creek, Manning River	SBE	13.12.23	0.429	30	3	24	1.37
7. Harrington, Manning River	SBE	14.12.23	0.720	40	3	38	1.37
8. Gerroa, Crooked River	IOCE	24.01.24	0.330	35	4	23	0.5, 1.0
9. Shoalhaven Heads, Shoalhaven River	SBE	24.01.24	0.655	15	2	28	1.37
10. Minnamurra, Minnamurra River	LBE	25.01.24	0.799	230	4	26	1.37
11. Lake Illawarra, Lake Illawarra	IOCE	25.01.24	0.099	45	4	32	0.5, 1.0
12. Silverwater Bridge, Parramatta River	DRV	26.01.24	1.095	45	4	30	1.37

1. Mean tidal range is the annual average difference in elevation between Mean Low Water and Mean High Water (MHL, 2024).
2. The cross-shore forest width refers to the distance from the seaward to landward extent of the mangrove forest. This width is measured in line with cross-shore transects, or at the midpoint of scans locations where scans were taken parallel to the shoreline.

Fig. 1 Locations and photos from the studied mangrove sites. **a** Site map with numbered icons corresponding to the TLS sites listed in the table; photos highlighting the diversity of forest structure for each estuary typology: **b** Site 1 (Middle Harbour South (DRV)), **c** Site 10 (Minnamurra, Minnamurra River (LBE)), **d** Site 7 (Harrington, Manning River (SBE)), and **e** Site 8 (Gerroa, Crooked River (IOCE))

2) Large Barrier Estuary (LBE), characterised by narrow or constrained downstream confluences that attenuate tidal wave propagation, with upstream areas of tidal amplification (Morris et al., 2013).
3) Small Barrier Estuary (SBE), characterised by restricted downstream confluences with tidal wave dampening often due to sand barriers forming at the entrances, and a constant flattening or decrease in the tidal plane (Morris et al., 2013).
4) Intermittently Open and Closed Estuary (IOCE), characterised by an entrance that is semi-permanently open (Kennedy et al., 2020), acting as a barrier estuary when open, and separated from all tidal dynamics when closed.

Within these estuary typologies, site locations were chosen based on their proximity to long-term water level tide gauges (Manly Hydraulics Laboratory, 2024), site accessibility, and to include both sand and marine clay sediment types. Almost all sites consist solely of grey mangroves (*Avicennia marina*), which have vertical pencil-shaped aerial roots called pneumatophores, enabling ease of comparison between sites. Based on available historical aerial imagery, many of the assessed forests have remained intact and undisturbed for at least 40 years.

The diversity of mangrove characteristics within these forests highlights the applicability of this method to other types of mangrove forests. In the studied forests of DRVs, visual observations of individual *Avicennia marina* mangroves revealed tall stems and high canopies (Fig. 1b). The pneumatophore root systems in these forests were dense with limited space for seedlings. In LBEs, forests were observed to have similarly tall trees and dense root systems, but with less consistent canopy heights than in DRVs (Fig. 1c). The elevation of the canopy varied from tree to tree in SBEs, and mangroves appeared as both shrubs and thinner, taller trees (Fig. 1d). A lower density of pneumatophores and large trees was observed together with a higher density of seedlings and saplings. Some mangroves in SBEs grew stilt roots or aerial cable roots from the sides of the stems. In IOCEs, mangroves mostly resembled multi-stemmed shrubs, with consistently low canopies extending from the ground to the top of the tree (Fig. 1e). In sandy IOCEs, pneumatophore density appeared lower than at other sites, while seedling density appeared higher. Like some of the mangroves in SBEs, older mangroves in IOCEs grew aerial stilt roots from the stems, but with much larger stem diameters. Details on each location are presented in Fig. 1.

Data Collection

At each site, a TLS device (FARO Focus^{M} 70 laser scanner (FARO, 2017)) was used to capture the stems, canopies, and root systems of the *Avicennia marina* forests. The FARO laser scanner has a range of 70 m, laser class 1, a maximum vertical scan speed of 97 Hz, a 300° vertical and 360° horizontal field of view, and a weight of 4.2 kg (FARO, 2017), complying with the minimum recommended requirements for the use of TLS in typical forest inventory applications (Maas et al., 2008). As per the manufacturer specifications, the FARO Focus^{M} 70 has a ranging error of ± 3 mm for distances up to 25 m (FARO, 2017), with greater inaccuracies for points beyond these distances. If the FARO laser scanner is not perfectly horizontal, a levelling of each scan was automatically performed by a dual axis compensator to an accuracy of 19 arcsec valid within $\pm 2°$ (FARO, 2017).

The TLS device was set up on a tripod at an elevation of approximately 1.8 m above the ground with a distance of at least 2 m to the surrounding trees to avoid immediate occlusion of trees by those nearest to the TLS device. In dense forests, the tripod was placed where the representative stem density of the forest could still be quantified, but with as much space as possible between the TLS device and neighbouring trees to meet the 2 m distance. Preliminary scans with durations of approximately 12 min (resolution of 174.8 MPts and 2× quality) and 30 min (resolution of 174.8 MPts and 4× quality) yielded point clouds of similar quality for trees within 15–20 m of the TLS device. Therefore, to minimise the time taken in the field, particularly as the low tide window was constrained to 2–3 h, a scan duration of approximately 12 min was adopted. A summary of these settings is presented in Fig. 2a. Scans were carried out as near to low tide as possible to minimise the reflections from water on the ground, as the presence of water distorted the recorded point clouds.

Data were collected in December 2023 and January 2024 by generating 2–4 scans with the TLS device along a transect in the cross-shore direction. Where forest widths were greater than 50 m, cross-shore transects were chosen to test the applicability of the method to both the landward and seaward forest extents. In forests with cross-shore widths smaller than 50 m, scans were taken parallel to the shoreline. The number of scans taken at each site was determined by the available time at low tide, and the forest width (Fig. 1). Each scan was separated by approximately 30 m to maximise the quality of the point cloud because trees within 15–20 m of the TLS device (approximately the midpoint of two TLS device locations) were observed to contain a greater number of points in the point cloud, due to the reduced occlusion of trees at this distance. However, due to the high density of trees at some sites, and the need to locate the TLS device where most trees could be observed, the 30 m separation distance could not always be adopted between adjacent scans. Therefore, distances from 22 to 40 m on average were adopted instead.

To validate the physical properties calculated from the point cloud scans, hand measurements of mangrove dimensions were taken with callipers, tape measures, and rulers.

a TLS Setting	Value
Resolution	174.8MPts (1/2)
Quality	2x
Scan duration	11m54s
High Dynamic Range (HDR)	Exposure bracketing 2x
GPS	On
Selected profile	Outdoor 20m
Field of view (vertical/horizontal)	300°/360°

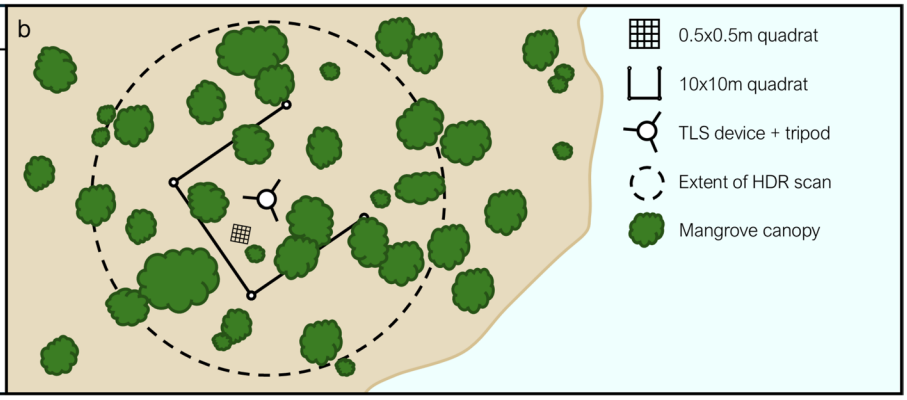

Fig. 2 Field data collection setup including **a** TLS parameter settings and **b** schematic of the fieldwork setup, TLS device, tripod, and quadrats

At each scan location, a 10 × 10 m quadrat was established by connecting the available 30 m tape measure around trees to form three sides of the quadrat (Fig. 2b). Within each quadrat, the number of stems was counted and divided by the quadrat area to determine the stem density. Measurements of the stem diameter at breast height (DBH), approximately 1.37 m from the ground (Kauffman & Donato, 2012), were obtained for 10 randomly selected trees within the quadrat. For two IOCEs (Crooked River and Lake Illawarra), where trees were shorter and stems often split into several branches at low elevations, the stem diameter was measured at elevations of 1.0 m and 0.5 m above ground. Due to difficulties in obtaining tree heights manually in dense forests, tree height measurements were focused on the Crooked River site, where trees were less than 3 m tall. Within each 10 × 10 m quadrat, a smaller 0.5 × 0.5 m quadrat was randomly placed in areas with minimal debris and fewer seedlings, to obtain information on the mangrove root structure (Fig. 2b). Within this 0.5 × 0.5 m quadrat, pneumatophore counts, and the diameters and heights of 10 randomly selected pneumatophores, were manually recorded.

Data Processing

To generate and process the TLS point cloud scans of the mangrove forests, the FARO SCENE (version 1.0.11127) (FARO, 2023) and CloudCompare (version 2.13) (2023) desktop software were used. FARO SCENE was used to load the scan files (.fls) from the FARO laser scanner and to load and apply the RGB values, which are included in the standard settings of the FARO laser scanner, to the point cloud. The resultant point cloud was exported in.xyz format and imported into CloudCompare (Fig. 3a). In CloudCompare, the vertical extents of the scan were trimmed with the Cross Section tool to remove any outliers that were disconnected from the main point cloud. A smaller 10 × 10 m point cloud around the FARO location (Fig. 3b) and three 0.5 × 0.5 m plots of pneumatophores were created by trimming the larger point cloud (Fig. 3c). These plots were close to, but not in direct alignment, with the locations of the quadrats in the field due to difficulties with identifying the GPS coordinates of the quadrat corners in the field. Therefore, for validation purposes, these smaller point clouds were used to reduce computational effort and compare the average values of the calculated mangrove attributes to the average values manually measured in the field. This process was repeated for all scans.

Physical Attributes

Physical attributes of individual *Avicennia marina* trees and forests (Fig. 4a) were quantified from the point cloud data using Python (version 3.10). These attributes inform a range of common parameters considered in the quantification of ecosystem services (Fig. 4b). The full set of Python scripts are available at https://zenodo.org/records/15009974.

Stem Density and Diameter

The stem density (n_{stem}) in each 10 × 10 m area scan was determined by dividing the number of identified stems by the area. The number of identified stems refers to the number of correctly calculated stem diameters (D_{stem}), which were identified by the circle fitting method based on the least squares fitting of algebraic surfaces (Pratt, 1987). This method was applied to clusters of points at the elevations specified in Fig. 1, with a vertical tolerance of 0.01 m. This circle fitting approach was previously applied to mangrove stems (Kargar et al., 2020), despite the cross-sections of tree stems typically exhibiting elliptical shapes (Kankare et al., 2013). Individual clusters of points were detected and filtered for their suitability using five user-defined thresholds (Note S1 of the Supporting Information). If the data point clusters from partially occluded stems satisfied these user-defined thresholds, a stem was still identified.

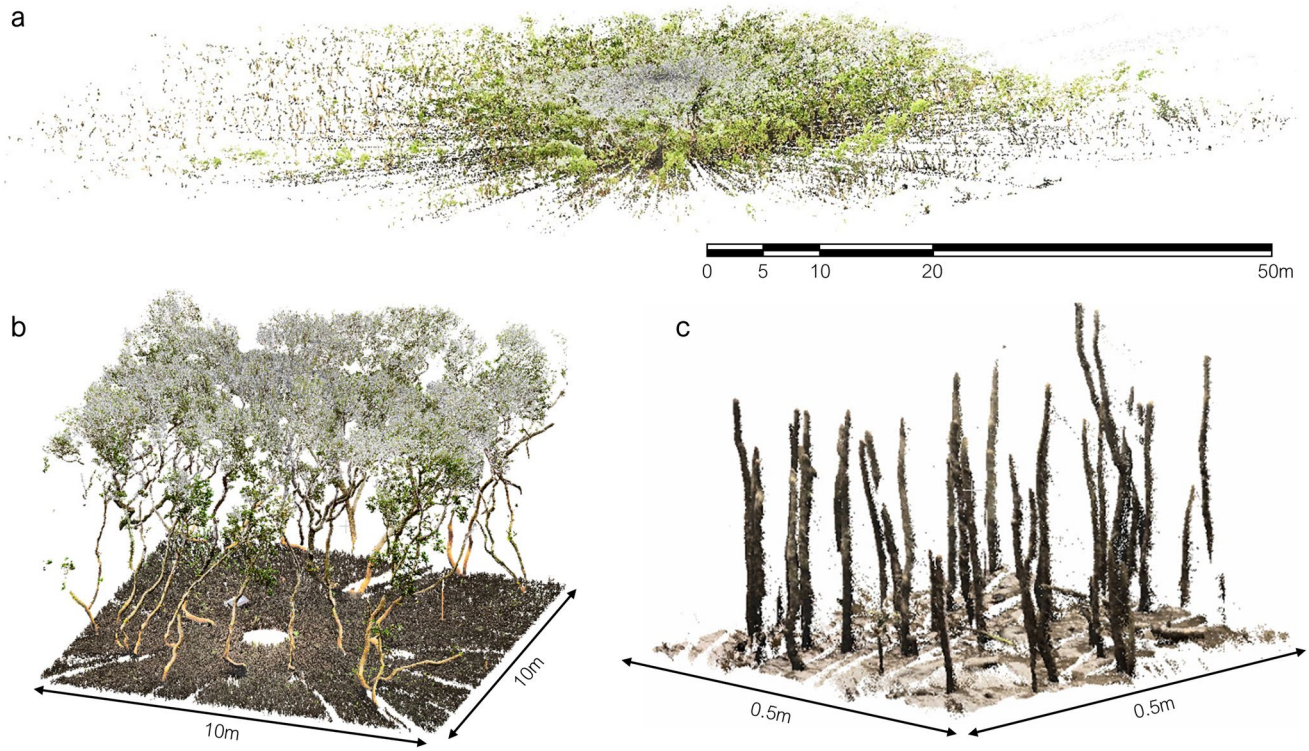

Fig. 3 Point cloud screenshots. **a** Full forest scan (Site 10, Minnamurra), **b** 10 × 10 m forest plot (Site 10, Minnamurra), and **c** 0.5 × 0.5 m pneumatophore plot (Site 8, Gerroa)

For further refinement, minimum and maximum radii were included to avoid erroneous circle fitting amongst dense clusters of points that do not correspond to individual trees, such as those from collections of leaves, branches, or other debris. These radii thresholds were cross-checked with the manual field data at each site. The range of values adopted for the stem identification and D_{stem} calculation filters are presented in Table S1 of the Supporting Information.

Following tree identification, the circle fitting method was carried out to fit a circle with centre co-ordinates and a radius to each cluster of points for a 10 × 10 m plot around the TLS device location for each scan (Fig. 5a). To validate these results, all fitted circles with their clusters of points, radii, and circle centres were plotted as cross-sections both on an area plot (Fig. 5b) and individually (Fig. 5c) for manual cross-checking with tree locations in the point cloud. The radius and subsequently D_{stem} of each tree were calculated, and the average value of all diameters in the plot was compared to the average value of diameters manually measured in the field.

Tree Height

Mangrove tree heights (H_{tree}) vary depending on their level of maturity (Salmo et al., 2013). This variation in H_{tree} was less pronounced for forests of younger mangroves, which are yet to experience competition from one another and for forests with older mangroves with stabilised growth patterns (Salmo et al., 2013). Leaning trees or trees differing from an idealised vertical profile may have canopies that lie below the main forest canopy elevation. For this reason, two techniques were tested to determine H_{tree}. The first technique calculated the maximum z-value of the 10 × 10 m forest plot. The second technique assumed that the centre of the fitted circle for D_{stem} was the centre of the tree stem and the maximum z-value within a 0.5 m radius from the centre of the circle was taken. H_{tree} was calculated as the difference between the maximum z-value and minimum z-value. The average H_{tree} for each scan was calculated using both techniques, and the results were compared to one another and to field measurements at Site 8, Gerroa (Fig. S1 in Supporting Information).

Sensitivity Analysis

The average values of mangrove stem attributes were calculated from the 10 × 10 m plots centred around the TLS device location and compared to manual field measurements. However, the locations of these 10 × 10 m plots may not adequately capture the morphological diversity within each forest. To identify the number of 10 × 10 m plots (n) required to achieve a convergent average D_{stem}

a

Notation	Attribute
D_{stem}	Stem diameter
n_{stem}	Stem density
H_{tree}	Tree height
D_{pne}	Pneumatophore diameter
n_{pne}	Pneumatophore density
H_{pne}	Pneumatophore height
A_{proj}	Projected area

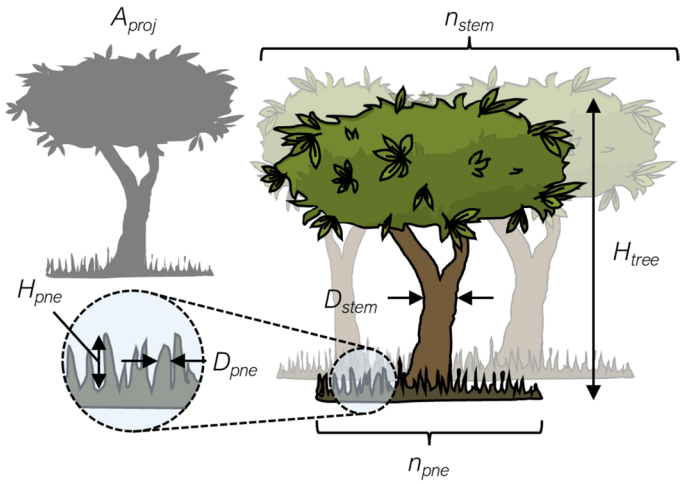

b

Service	Parameter	Notation	Mangrove attribute						
			D_{stem}	n_{stem}	H_{tree}	D_{pne}	n_{pne}	H_{pne}	A_{proj}
Climate change mitigation	Aboveground biomass	*AGB*	✓		✓	●	●	●	
	Belowground biomass	*BGB*	✓						
Climate change adaptation	Drag coefficient	C_d	✓	✓	✓	✓	✓		✓
	Bulk roughness	C_b	✓	✓		✓	✓	✓	
	Damping coefficient	β	✓	✓		✓	✓	✓	✓

✓ Attribute captured in available equations
● Attribute proposed for use in future equations

Fig. 4 Physical attributes of mangrove forests calculated from TLS point cloud data. **a** Diagram of mangrove trees with annotated attributes. **b** Mangrove attributes required for common parameters considered in the quantification of ecosystem services

and H_{tree}, a sensitivity analysis was undertaken. This analysis involved forming unique 10 × 10 m plots with randomised centre coordinates for $n = 1$ to $n = 10$. The centre coordinates of these plots were determined randomly using Python and restricted such that the boundaries of these plots were within a set distance of the TLS device location to maximise point cloud density and did not overlap with one another. This random sampling was undertaken for one of each estuary typology, except for IOCEs, because the density of the foliage in IOCEs constrained the quality of the scans to a localised radius of around 10 m from the TLS setup.

The values of D_{stem} and H_{tree} were calculated for all trees in the 10 × 10 m plots. Two statistical tests were applied to determine the required value of n to achieve convergent average D_{stem} and H_{tree} values for each forest scan. The analysis of variance (ANOVA) was employed to evaluate whether any significant difference existed between the means of the distributions for all values of n. If the test revealed a significant difference (p-value < 0.05) in the means for $n = 1$ to $n = 10$, then the Tukey honestly significant difference (HSD) test (Tukey, 1949) was applied to determine the values of n that were significantly different.

Pneumatophores

Pneumatophores were identified in the point cloud using the same circle fitting approach as the stems. This approach was applied to pneumatophores within three 0.5 × 0.5 m plots (Fig. 6a) to determine the density (n_{pne}), diameter (D_{pne}), and height (H_{pne}) of individual roots. Like the stems, user-defined thresholds were applied to filter the clusters of points for accurate pneumatophore identification (Note S1 of the Supporting Information). Fewer thresholds were applied to the pneumatophores than for the stems because of the difficulty with filtering irregular point cloud clusters caused by the presence of marine growth and debris on the pneumatophores. The full set of filter values for each scan and pneumatophore plot is presented in Table S2 of the Supporting Information.

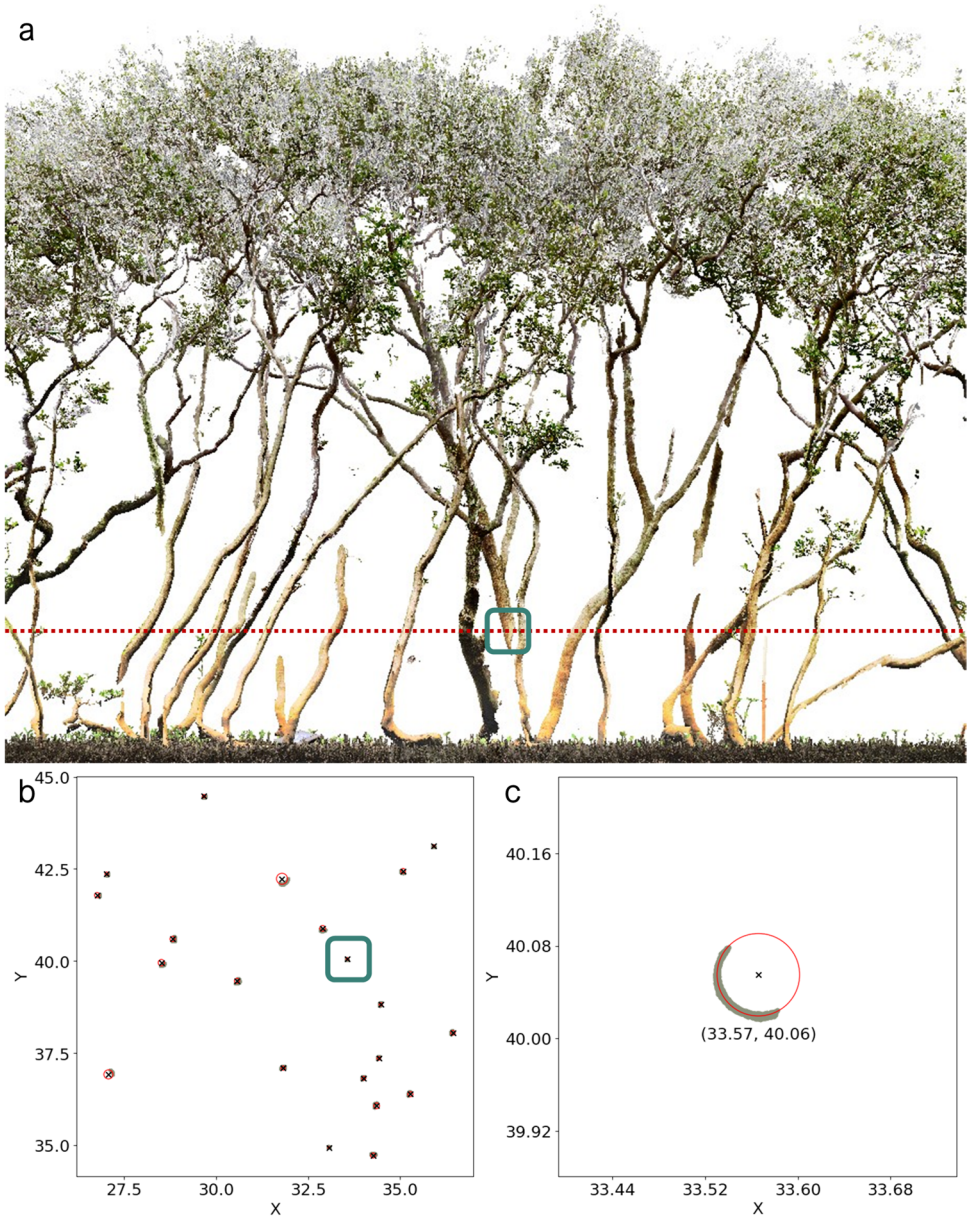

Fig. 5 Circle fitting of stems at Site 10 (Minnamurra, Minnamurra River (LBE)). **a** Side view of the 10 × 10 m plot with the z-plane of D_{stem} measurements shown with a dashed red line (1.37 m elevation). **b** Plan view of the circle fitting of all stems identified within the 10 × 10 m plot. **c** Plan view of the circle fitting for the individual stem marked in (**a**) and (**b**)

The elevation of the z-plane for identifying pneumatophores and their diameters was taken to be one third of the tallest pneumatophore within the plot. This level was selected because it was found to be low enough to increase the opportunity for small pneumatophores to be detected, but high enough such that clumps of sediment and debris were ignored. Like the stems, minimum and maximum radii tolerances were applied to limit extreme values. The number of pneumatophores identified within each plot was then divided by the area of the plot (0.5 × 0.5 m), to determine n_{pne}. Examples of the circle fitting results of all pneumatophores, and of a single pneumatophore, within one 0.5 × 0.5 m plot, are shown in Fig. 6b and c, respectively.

In each plot, H_{pne} values were calculated by subtracting the minimum z-value of the pneumatophore plot from the maximum z-values above the diameter centres of the pneumatophores. A radius tolerance of 0.004 m was used to ensure that the maximum z-value above the centre of the pneumatophore could also be determined for leaning pneumatophores.

Projected Area

The projected area (A_{proj}) refers to the projection of the three-dimensional mangrove point cloud onto a two-dimensional arbitrary plane. The value of A_{proj} was calculated by applying an alpha shape parameter of 0.01 (Kalloe et al., 2022) to define a bounding polygon around the point cloud. The area covered by the points within the polygon was calculated and plotted against the elevation. For computational efficiency,

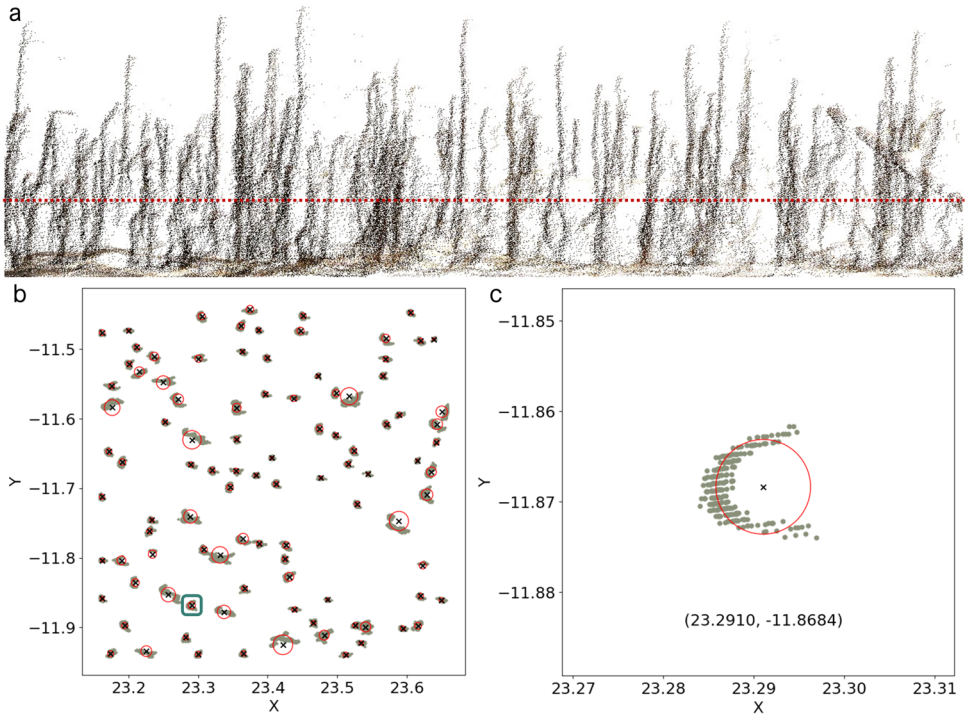

Fig. 6 Pneumatophore properties at Site 1 (Middle Harbour South (DRV)). **a** Side view of a 0.5 × 0.5 m pneumatophore plot with a dashed horizontal line representing the *z*-plane at which the circle fitting method was applied. **b** Plan view of the circle fitting of all pneumatophores in the 0.5 × 0.5 m plot. **c** Plan view of the circle fitting for the individual pneumatophore marked in (**b**)

the alpha shape for the 10 × 10 m mangrove forest plots was computed by separating the point cloud into 1 m slices along either the *x*- or *y*-planes and aggregating the areas at the end. The area of the alpha shape in the *z*-plane was then determined by summing the area of vertical layers with a constant user-defined width. Surface area measurements were not taken in the field, and thus, the projected areas have not been validated. Projected alpha shape and projected area plots of a 10 × 10 m forest, an individual mangrove tree, and a 0.5 × 0.5 m pneumatophore plot, are presented in Fig. 7.

Results

Stems

Identification and Validation

In DRVs and LBEs, the calculated stem density (n_{stem}) in each 10 × 10 m plot closely matched the measured n_{stem} (Fig. 8a). The difference between calculated and measured results was within ± 5% for scans at Sites 1, 2, 4, and 12, with perfect agreement for some scans at Sites 1, 2, 4, and 10. This is largely due to the greater similarity in vertical profiles of trees within these forests, where branches and foliage are constrained to higher elevations and thus are not obstructing the view from the TLS device to the stems. However, some scans in DRVs and LBEs contained a higher density of foliage, where clusters of branches and leaves could be mistakenly identified as stems. This increased the average discrepancy between the calculated and measured n_{stem} to ± 13%. For sites with many smaller trees comprising branches and foliage that occlude other tree stems, such as those in SBEs and IOCEs, the calculated n_{stem} also matched the measured n_{stem} for some scans (e.g. at Sites 5 and 7), but was, on average, within ± 42% of the measured n_{stem}. Across all scans, stem identification accurately filtered out leaves and debris with an accuracy of 87% and 97% when IOCEs were excluded.

The average calculated stem diameter (D_{stem}) varied from the average D_{stem} measured in the field due to trees typically exhibiting an elliptical rather than circular cross-section and where tree stems were relatively more oblique. Larger calculated D_{stem} averages than those in the field were observed because the circle fitting method is based on a horizontal plane for D_{stem} calculation, rather than taking D_{stem} perpendicular to the stem edge. This led to larger D_{stem} values for leaning stems, especially those that inclined more than 25° from the vertical (Fig. 9a). Despite these differences in shape, diameter estimates showed good agreement with field measurements. Differences between the calculated and the measured results were lower in some estuary typologies than others (Fig. 8b), with larger deviations in estuaries with greater variation in tree ages and sizes. Across all scans in DRVs, the difference between calculated and measured D_{stem} was ± 10% on average, with ± 2% differences for some scans at Sites 1 and 2. The discrepancy in IOCEs and barrier estuaries was on average within ± 37% and ± 46%, respectively, but as low as ± 2% at Site 6. Mangrove forests in these

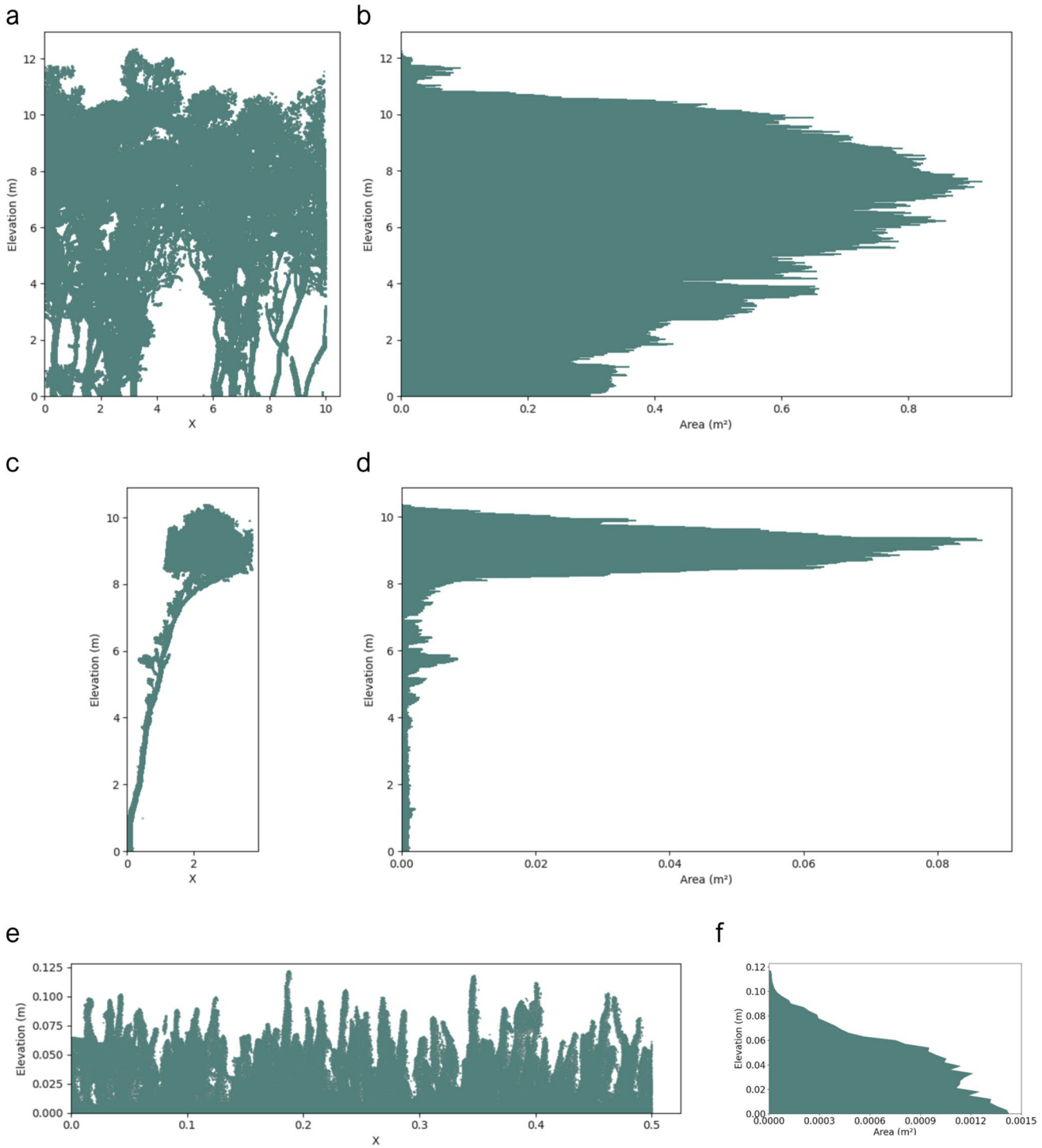

Fig. 7 Projected area of mangroves. **a** Alpha shape projection and **b** projected area profile of a 10 × 10 m mangrove plot at Site 2 (Spencer, Hawkesbury River (DRV)). **c** Alpha shape projection and **d** projected area profile of an individual mangrove tree at Site 1 (Middle Harbour South (DRV)). **e** Alpha shape projection and **f** projected area profile of a 0.5 × 0.5 m pneumatophore plot at Site 1 (Middle Harbour South (DRV)). Note that pneumatophores are excluded from the projections for the 10 × 10 m and individual tree plots for clarity

estuaries comprised stems of varied ages and sizes, where smaller stems were not detected clearly using TLS. For this reason, when the 10 mangroves measured in the field included saplings or small trees, the average measured D_{stem} was often lower than the average calculated D_{stem} of all trees in a point cloud scan.

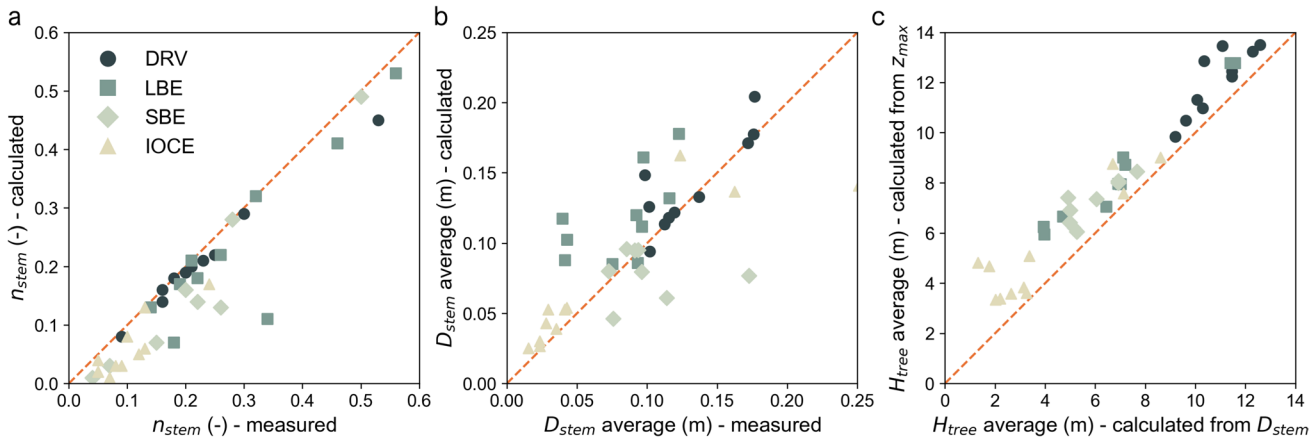

Fig. 8 Accuracy of stem identification and attribute calculations for **a** stem density (n_{stem}); **b** stem diameter (D_{stem}); and **c** tree height (H_{tree})

Like D_{stem}, tree heights (H_{tree}) varied across all estuary types. The average H_{tree} calculated at the location of D_{stem} (i.e. at the locations of the circles in Fig. 5b), differed from the maximum z-value of the 10 × 10 m plot on average by up to ± 11% in DRVs, ± 25% in barrier estuaries, and ± 65% in IOCEs. On average, this discrepancy was within ± 34% across all forest scans (Fig. 8c). Using the maximum z-value of the forest plot is likely only suitable in lieu of other data for forests with consistent vertical profiles. The maximum z-value typically overstated H_{tree} within the forest but provided a suitable estimate in forests with trees of similar ages and profiles. In forests where mangrove stems exhibited greater degrees of inclination, a larger difference was observed between the maximum z-value of the forest and the average H_{tree} calculated using the location of D_{stem} (Fig. 9b). When comparing H_{tree} results calculated via the D_{stem} locations with values manually measured at Site 8 (Gerroa, Crooked River (IOCE)), the average H_{tree} was within ± 17% of the measured values (Fig. S1 of the Supporting Information).

Sensitivity Analysis

By comparing the calculated results to those manually measured in the field, the number of 10 × 10 m plots needed to represent the forest can be determined. The sensitivity analysis revealed that 1–2 plots are required to characterise a forest area of 400–1300 m^2 and to achieve convergent mean D_{stem} and H_{tree} values (Fig. 10). These findings were statistically confirmed with the combined ANOVA and Tukey

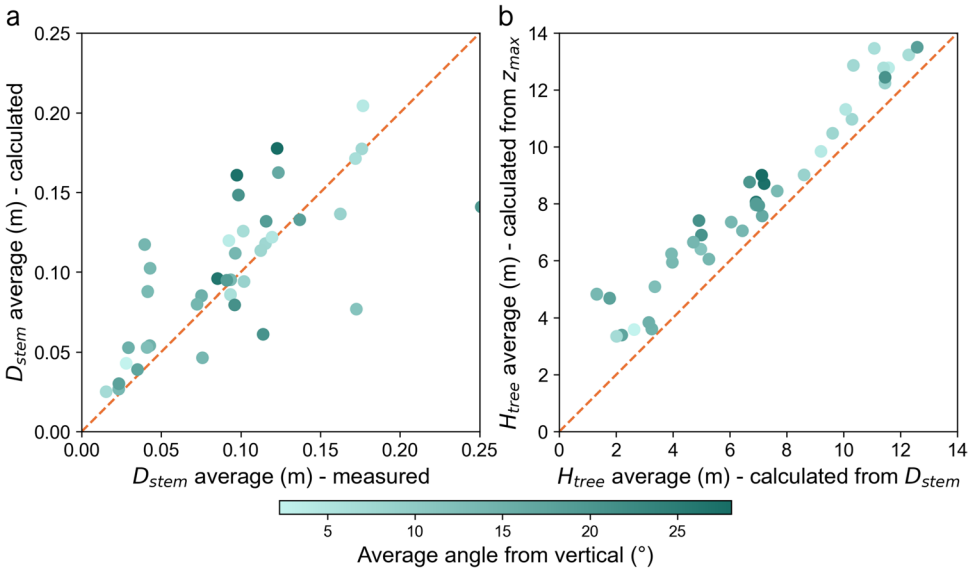

Fig. 9 Influence of stem angle on the accuracy of **a** stem diameter (D_{stem}) estimations and **b** comparison of tree height (H_{tree}) measurement techniques

HSD tests. Only one plot (10–20 trees) would be required for the observed forest morphologies in Site 1 (Middle Harbour South (DRV)) (Fig. 10a and b) and Site 7 (Harrington, Manning River (SBE)) (Fig. 10e and f). However, for Site 4 (Kooragang Island, Hunter River (LBE)) (Fig. 10c and d), one plot would be required for D_{stem} and two for H_{tree}. It is therefore recommended that two plots (corresponding to 35–45 trees) are considered for barrier estuaries due to the diverse forest structures in these estuaries. Similarly, when processing point cloud scans for the calculation of D_{stem} and H_{tree}, a larger plot size, closer to 20×10 m, is recommended to obtain values representative of the forest.

Pneumatophores

Pneumatophore density (n_{pne}) manually measured in the field was greater than the calculated n_{pne} for all scans and estuaries (Fig. 11a). Small pneumatophores that could be identified by eye were often not picked up by the scan nor the algorithm for detecting pneumatophore root diameters. Further, pneumatophores that grew adjacent to one another were sometimes identified by the algorithm as a single root instead of multiple roots. However, for the detected pneumatophores, the calculated average D_{pne} was within $\pm 4\%$ of the measured D_{pne} at some sites (e.g. Sites 8 and 9) but increased to $\pm 54\%$ when averaged across all sites (Fig. 11b). The resultant values presented a distribution where most values of D_{pne} were between 6 and 10 mm, indicating that measurements from either the field or with TLS produce results that typically differed by only a few millimetres. Larger diameters observed with TLS were due to the presence of heavy marine growth, especially at sites with smaller pneumatophores that could not be separated visually from one another by the TLS device. The average D_{pne} calculations for IOCEs resulted in lower values when compared to the manual measurements, indicating that TLS captured thinner and smaller roots when the pneumatophore density was lower.

The pneumatophore height (H_{pne}) calculations closely matched the measured results for smaller heights but were lower than those measured in the field for larger heights (Fig. 11c). This may be attributed to subconscious bias when selecting pneumatophores to sample in the field, where larger pneumatophores may be chosen. Further, only 10 pneumatophores were sampled in the field at each scan site, whereas the method utilised here calculated the

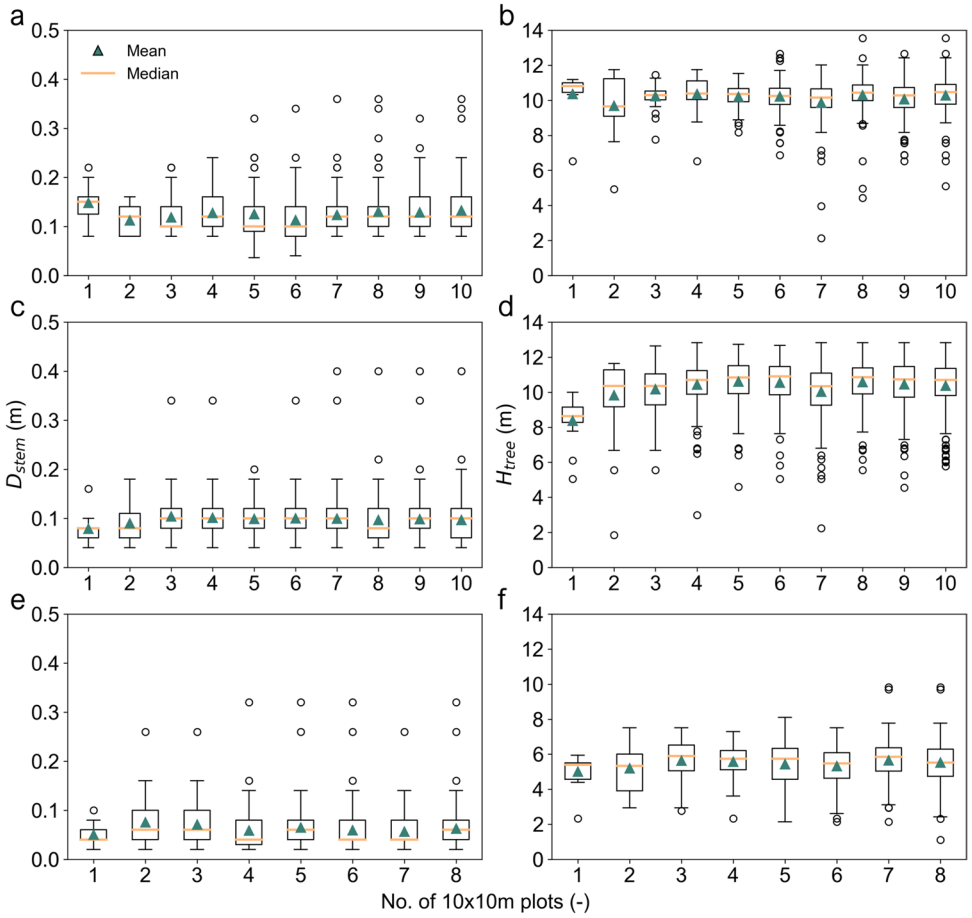

Fig. 10 The spread of stem diameter (D_{stem}) and tree height (H_{tree}) results determined from "n" randomly sampled 10×10 m plots in a single forest scan. **a** Stem diameter (D_{stem}) and **b** tree height (H_{tree}) for Site 1 (Middle Harbour South (DRV)); **c** stem diameter (D_{stem}) and **d** tree height (H_{tree}) for Site 4 (Kooragang Island, Hunter River (LBE)); and **e** stem diameter (D_{stem}) and **f** tree height (H_{tree}) for Site 7 (Harrington, Manning River (SBE))

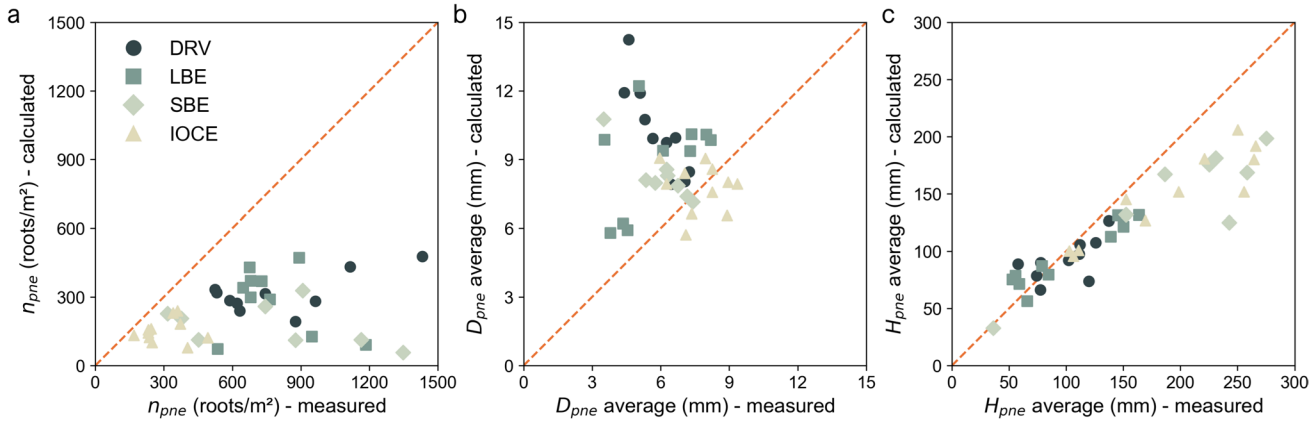

Fig. 11 Average pneumatophore properties manually measured in the field compared to the values calculated from three point-cloud plots of 0.5 ×0.5 m for each scan. **a** Pneumatophore density (n_{pne}); **b** pneumatophore diameter (D_{pne}); **c** pneumatophore height (H_{pne})

average height for all 50–100 detected pneumatophores within the 0.5 ×0.5 m plot and inherently calculated a lower average H_{pne} where smaller pneumatophores were detected. H_{pne} was on average within ±20% of the measured H_{pne} for all estuaries. For DRVs, the calculated H_{pne} was on average within ±18%, and ±21% of the measured H_{pne} for other estuary types.

Projected Area

The total A_{proj} for the 10 ×10 m plots was compared for 10 scans across Sites 1–3, yielding an average difference of less than ±5%. For individual trees, the average difference was less than ±9%. A_{proj} was calculated and compared for both *x*-*z* and *y*-*z* planes of 10 ×10 m mangrove forest plots and individual mangrove trees to assess the area that is directly impacted by environmental forcing of incident waves, currents, or wind. Observed differences in total area were minor (Fig. S2 of the Supporting Information), indicating that calculating A_{proj} in one plane only (either *x*-*z* or *y*-*z*) is sufficient for mangrove forest plots.

The A_{proj} profiles for the 10 ×10 m forest plots in the *x*-*z* plane highlighted the differences between scans in the same mangrove forest (Fig. 12). These differences aligned with the elevations of canopies, such as above an elevation of 4 m at Site 1 (Middle Harbour South (DRV)) (Fig. 12a) and below an elevation of 1.5 m at Site 8 (Gerroa, Crooked River (IOCE)) (Fig. 12b). As the diversity of the forest structure increased from more consistent forests in terms of size in DRVs to forests that varied in terms of age and size in barrier estuaries and IOCEs, the alpha shape projections varied. These results demonstrate the need to consider the type and location of the site within the mangrove forest prior to performing the projected area analysis. Such an analysis may also be used to compare the distribution of mangrove forest profiles across estuaries (Fig. 12c and d).

Discussion

Forest Dynamics and Restoration Management

The introduced method using TLS has demonstrated success in capturing the density and diameter of mangroves in estuaries and coastal settings. In estuary typologies such as IOCEs, smaller trees and the presence of dense foliage suggests alternative techniques (e.g. hand sampling) may be required to complement the method presented. These measurements, if taken periodically, can help practitioners evaluate the temporal forest dynamics by developing allometric relationships to assess whether the site is growing (increase in diameter), recruiting new seedlings (increase in density), or dying (reduction in density or stagnation of growth) (Dunlop et al., 2023). In addition to the recruitment and growth of the forest, the resilience to extreme events can also be determined by comparing the physical attributes of mangroves. For example, calculations of pneumatophore dimensions before and after flood events can inform both pneumatophore growth rates in periods of stress and the resilience of the forest to adapt to increasing pressures. By monitoring the change in mangrove attributes and assessing the dynamic responses to climate pressures, health indicators and restoration trajectories can be quantified, and management strategies can be tailored to the site and estuary typology (Asbridge et al., 2024).

Climate Change Mitigation and Adaptation

The ecosystem services of carbon storage and coastal protection can similarly be quantified via the physical attributes measured with this method. Existing biomass equations can be used to calculate the carbon stored within a mangrove ecosystem using the attributes of D_{stem} and H_{tree}. Measuring pneumatophores can also lead to an expansion of the current state of knowledge, where terms associated

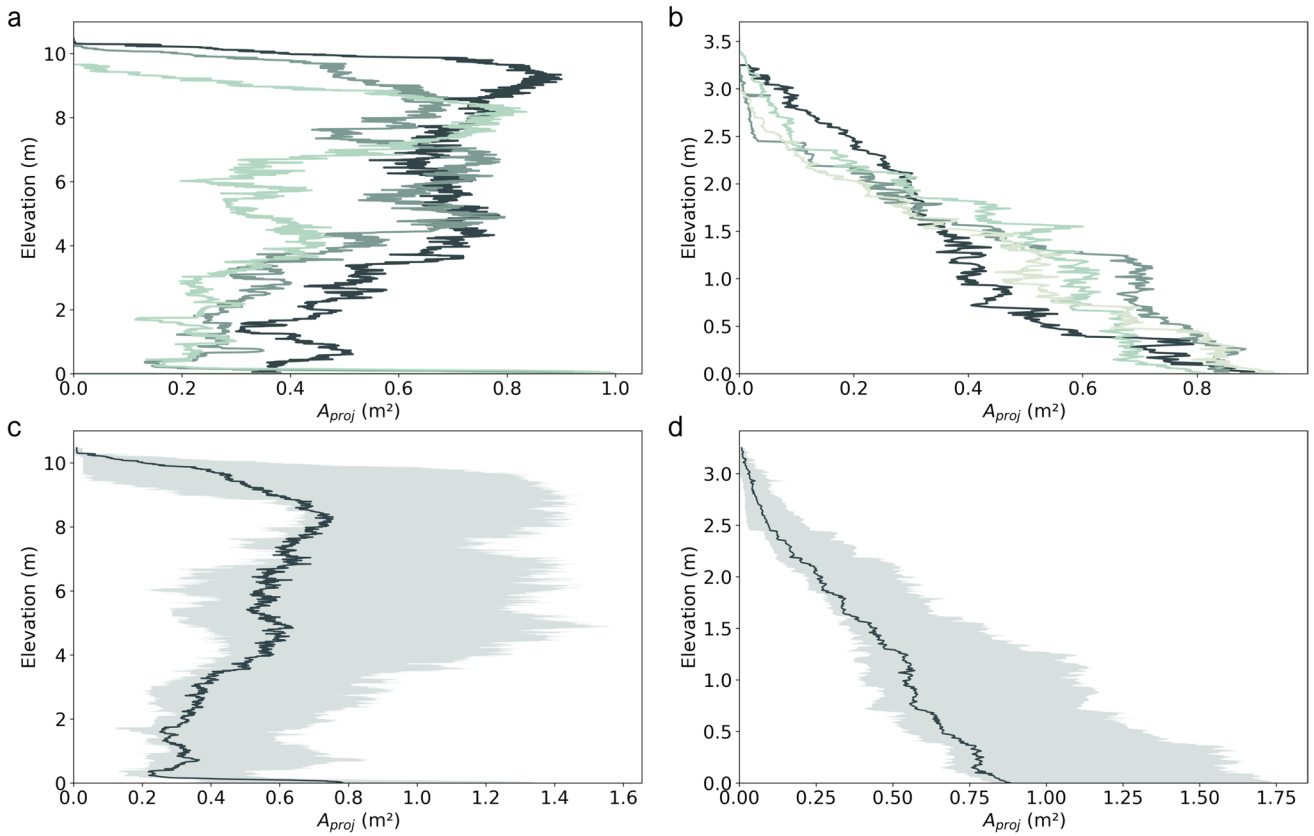

Fig. 12 Vertical projected area (A_{proj}) profiles of 10 × 10 m mangrove forest plots for scans at **a** Site 1 (Middle Harbour South (DRV)) and **b** Site 8 (Gerroa, Crooked River (IOCE)). Range of projected area profiles (coloured hatch) and mean profile (dark solid line) for **c** Site 1 (Middle Harbour South (DRV)) and **d** Site 8 (Gerroa, Crooked River (IOCE))

with the aboveground root system can be captured in AGB calculations.

Quantifying mangrove attributes is also helpful in assessing mangrove restoration for coastal protection services. Existing difficulties in obtaining site specific data can lead many practitioners to adopt simplified wave attenuation rates from available literature, where modelling is typically based on one tree. However, as found in this study, the physical attributes of mangrove trees can vary significantly from site to site. For example, the calculated n_{stem} varied across the surveyed estuaries from 0.01 ot 0.50 stems/m^2 and the average D_{stem} varied from 0.03 to 0.22 m. Further, the mangrove forest projected area profiles differed from those of single trees. By observing how the vertical profiles of the forests change, a more detailed representation of mangroves can be developed to replace simplified cylindrical models used in numerical and physical modelling. Practitioners can then compare these profiles with the elevations at which wind and wave forces act to calculate the forces on the forests or to determine whether mangroves can withstand extreme events (Gijón Mancheño et al., 2024). In this way, numerical models could be developed based on the field measurements to predict how existing and restored mangrove sites will respond to storm forces.

Mangrove Genera and Estuary Typologies

In this method, the steps required to post-process the field data for mangrove stems are expected to be applicable to other mangrove genera. Calculations of pneumatophore attributes are likely to be more applicable to mangroves with pencil-type roots, such as *Avicennia* sp., *Sonneratia* sp., and *Laguncularia* sp., where the height of the roots can be measured in the same way as the stems. Aerial root identification and diameter calculations may also be applicable to mangrove genera with stilt roots (e.g. *Rhizophora* sp.), because these roots exhibit an elliptical or circular cross-section, but less applicable to those with buttress roots (e.g. *Ceriops* sp.) or knee roots (e.g. *Bruguiera* sp.), which have irregular cross-sectional profiles. The diversity in forest structure of the studied mangrove sites, and the high reliability of stem detection across a range of canopy elevations and stem densities, means that the proposed TLS method will also be applicable across genera if the stems can be clearly distinguished from the roots and canopy. This application may be more dependent on the environmental conditions at the site than the mangrove genus and species.

Like the mangrove genera, some forest types may be more suitable to the method proposed in this study. In forests with consistent tidal dynamics (DRVs), where individual mangroves have similar tree heights, stem diameters, and canopy elevations, the calculated vertical structure closely matched the field measurements. In estuaries with variable tidal forcing (barrier estuaries and IOCEs), where mangrove size varies, canopy heights are low, and the density of young thin trees is high, attribute calculations of forest structure may differ from field measurements. In these variable forest structures, sampling larger point cloud datasets (20×10 m) and taking additional hand measurements (35–45 trees) is advised for more accurate mangrove representation and improved validation. In forests where trees are strongly inclined, such as those in this study with angles above 25°, a volumetric approach to calculate stem diameters may be more accurate (Kargar et al., 2020; Owers et al., 2018). Such an approach could calculate the volume of the overall stem without the need to calculate D_{stem} in the horizontal plane, where D_{stem} may be overestimated. Where pneumatophore density is high, the point cloud data from the TLS device may be unable to distinguish between adjacent roots. Differentiating between roots may be more difficult in forests with multiple species and varying root types (e.g. *Rhizophora* sp. with stilt roots, *Sonneratia* sp. with pencil roots, and *Ceriops* sp. with buttress roots). Similarly, where marine growth is prevalent, TLS may overestimate pneumatophore diameters. In such forests, it is recommended to supplement TLS measurements with hand-based density measurements and to record the thickness of marine growth using callipers to ensure a true diameter can be calculated.

Improvement Opportunities

The new method proposed is constrained by the capability of the TLS device and the prevailing environmental conditions in the mangrove forests, where the post-processing algorithms rely on sufficient point cloud data to detect trees. In the field, the low tide window presents the best opportunity for scanning due to a reduced number of reflections from ponding. The low tide window is typically a few hours, and, in this method, a low scan duration of approximately 12 min was chosen to maximise scan accuracy while retaining a high level of resolution (3.1 mm resolution at 10 m). However, as TLS and handheld devices improve, high quality scans with shorter durations (< 1 min) (RIEGL, 2024) could be taken and co-registered (Olagoke et al., 2016) to achieve a complete point cloud, reducing the impact of the long installation times and narrow measurement ranges of current TLS devices. Higher capacity TLS devices would be useful in dense forests, such as in IOCEs where fewer trees can be observed in a single scan than in other estuary typologies.

Similarly, TLS device upgrades providing higher resolution and shorter scan times (FARO, 2024) may assist in detecting smaller branches. Small branches and foliage were difficult to capture in this study due to signal attenuation toward the upper canopy layers (Côté et al., 2009), especially when exposed to wind. When captured, small elements create scattered data that is difficult to process. Further, when calculating the height of the forest plots, isolating individual trees (Burt et al., 2019) could provide a more accurate approximation than taking a z-value at the top of the canopy. However, the complexity and density of each mangrove forest surveyed in this study has made it difficult to isolate trees using techniques applied to terrestrial forests, and thus approximate methods have been used. Alternative approaches may also be used to refine the proposed stem identification process. Filters defining the angle between the end points of each cluster (Kalloe, 2019) or the range of colour intensity values that can separate stems from leaves may further eliminate erroneous results and refine the identification of individual trees.

Additional research may also be carried out to expand on the proposed method for the calculation of stem height and subsequent canopy elevation extent. The tree height referred to the distance between the top of the canopy and the ground level. However, the thicker parts of the main stem of each mangrove tree, which have a greater impact on mitigating incident wave forcing than the leaves in the canopy (van Wesenbeeck et al., 2022), typically end below the canopy level. Therefore, deriving an algorithm that can detect where the canopy starts and ends in terms of elevation may more accurately quantify mangrove forest resilience. Similarly, developing a method that can effectively remove the leaves from the woody part of the mangrove forest (Burt et al., 2019; Owers et al., 2018; Wilkes et al., 2023) would reveal the proportion of the forest associated with flexible elements. Preliminary analyses of individual trees from the point cloud data discussed in this study have shown that leaf area factors can be derived based on a comparison of the projected area results, where leaves can be manually removed using CloudCompare in lieu of more sophisticated algorithms.

Conclusion

This study presented a novel method to quantify the physical attributes of mangrove forests from a point cloud obtained with a TLS device. Previous studies have investigated mangrove stem diameter and volume using TLS, but with considerable processing times associated with pre-training datasets for attribute classification. This method instead used TLS data to calculate a suite of parameters applicable to a range of ecosystem services, such as density, diameter,

height, and projected area of stems and roots, without the need to co-register scans nor manually classify mangrove attributes. Validation of this method was achieved with hand measurements from 12 *Avicennia marina* forests across four estuary typologies. Greater agreement was found for mangrove forests with greater consistency in size and age, such as those in DRVs. For mangrove forests with less consistent tides, such as those in barrier estuaries, approximately 35–45 trees would need to be measured by hand or processed using the TLS point cloud to calculate characteristics representative of the forest. Where foliage is dense at lower elevations, such as in the mangrove forests of IOCEs, TLS is less effective at detecting tree stems and processing data. Overall, this method demonstrates its applicability to wider mangrove genera and can be used by practitioners seeking to efficiently measure the physical attributes of mangrove forests worldwide.

Integrating this approach into mangrove restoration frameworks may assist with preliminary site investigations, where quantifying forest structure can influence the likelihood of successful restoration and the expected growth and geometric profile of restored mangroves. Following restoration works, TLS may be used to monitor mangrove attributes to quantify the success of the restored site in achieving the desired ecosystem services and in comparison to neighbouring forests. These datasets can complement global remote sensing observations of forest extent and canopy cover to form a baseline for future research and conservation strategies. TLS appears to be a valuable tool to form datasets of the understory attributes of mangrove forests across genera and biogeographic regions that can inform global mangrove conservation policies.

Supplementary Information The online version contains supplementary material available at https://doi.org/10.1007/s12237-025-01533-0.

Acknowledgements The authors thank Dana Lanceman (UNSW Sydney), Jayati Dave, and Toby Tucker (WRL, UNSW Sydney) for offering their time, support, and assistance in collecting the data in the field. The authors also thank Chantal Willems and Pieter van der Gaag (TU Delft) for their support setting up additional computing resources.

Author Contribution Thomas Dunlop and William Glamore conceptualised the study. Thomas Dunlop, Alejandra Gijón Mancheño, William Glamore, and Bregje K. van Wesenbeeck designed the data collection methodology. Thomas Dunlop and William Glamore conducted the field investigation. Thomas Dunlop and Alejandra Gijón Mancheño planned and designed the data processing methodology. Thomas Dunlop wrote the data processing codes and carried out the data analysis. Thomas Dunlop and Alejandra Gijón Mancheño designed the figures. Alejandra Gijón Mancheño, William Glamore, Stefan Felder, and Bregje K. van Wesenbeeck supervised the development of the paper. Thomas Dunlop wrote the original paper. All authors reviewed the methodology and edited and revised the paper.

Funding Open Access funding enabled and organized by CAUL and its Member Institutions.

Data Availability The Python code, an example mangrove forest point cloud, and data used to generate the figures in this paper can be accessed at https://zenodo.org/records/15009974.

Declarations

Ethics Approval and Consent to Participate Not applicable

Consent for Publication Not applicable

Competing Interests The authors declare no competing interests.

References

Alongi, D. M. (2014). Carbon cycling and storage in mangrove forests. *Annual Review of Marine Science, 6*, 195–219. https://doi.org/10.1146/annurev-marine-010213-135020

Asbridge, E., Clark, R., Denham, P., Hughes, M. G., James, M., McLaughlin, D., Turner, C., Whitton, T., Wilde, T., & Rogers, K. (2024). Tidal impoundment and mangrove dieback at cabbage tree Basin, NSW: Drivers of change and tailored management for the future. *Estuaries and Coasts, 47*(8), 2190–2208. https://doi.org/10.1007/s12237-024-01426-8

Bunting, P., Rosenqvist, A., Lucas, R. M., Rebelo, L.-M., Hilarides, L., Thomas, N., Hardy, A., Itoh, T., Shimada, M., & Finlayson, C. M. (2018). The global mangrove watch—A new 2010 global baseline of mangrove extent. *Remote Sensing, 10*(10), 1669.

Burt, A., Disney, M., & Calders, K. (2019). Extracting individual trees from lidar point clouds using treeseg. *Methods in Ecology and Evolution, 10*(3), 438–445. https://doi.org/10.1111/2041-210X.13121

Calders, K., Adams, J., Armston, J., Bartholomeus, H., Bauwens, S., Bentley, L. P., Chave, J., Danson, F. M., Demol, M., Disney, M., Gaulton, R., Krishna Moorthy, S. M., Levick, S. R., Saarinen, N., Schaaf, C., Stovall, A., Terryn, L., Wilkes, P., & Verbeeck, H. (2020). Terrestrial laser scanning in forest ecology: Expanding the horizon. *Remote Sensing of Environment, 251*, 112102. https://doi.org/10.1016/j.rse.2020.112102

Chave, J., Andalo, C., Brown, S., Cairns, M. A., Chambers, J. Q., Eamus, D., Fölster, H., Fromard, F., Higuchi, N., Kira, T., Lescure, J. P., Nelson, B. W., Ogawa, H., Puig, H., Riéra, B., & Yamakura, T. (2005). Tree allometry and improved estimation of carbon stocks and balance in tropical forests. *Oecologia, 145*(1), 87–99. https://doi.org/10.1007/s00442-005-0100-x

CloudCompare. (2023). 3D point cloud and mesh processing software. In (Version 2.13) http://cloudcompare.org

Côté, J.-F., Widlowski, J.-L., Fournier, R. A., & Verstraete, M. M. (2009). The structural and radiative consistency of three-dimensional tree reconstructions from terrestrial lidar. *Remote Sensing*

of Environment, 113(5), 1067–1081. https://doi.org/10.1016/j.rse.2009.01.017

Dunlop, T., Glamore, W., & Felder, S. (2023). Restoring estuarine ecosystems using nature-based solutions: Towards an integrated eco-engineering design guideline. *Science of The Total Environment, 873*, 162362. https://doi.org/10.1016/j.scitotenv.2023.162362

FARO. (2017). FARO® FocusM 70 Laser Scanner: Short-range professional grade laser scanner. https://downloads.faro.com/index.php/s/xPtkFj6R3TaCtFX?dir=undefined&path=%2FEarlier%20Versions&openfile=41328

FARO. (2023). FARO SCENE. In (Version October 2023) https://www.faro.com/en/Products/Software/SCENE-Software

FARO. (2024). FARO: Focus laser scanning solution. https://media.faro.com/-/media/Project/FARO/FARO/FARO/Resources/1_BROCHURE/2024/FARO-Focus/AECO/CMO9773_Brochure_FocusPremiumMax_AECO_ENG_LT_Web_112024.pdf?rev=32d2a3ce59b943828b19a6a2e5374d94

Faunce, C. H., & Serafy, J. E. (2006). Mangroves as fish habitat: 50 years of field studies. Marine Ecology Progress Series, 318, 1-18. https://www.int-res.com/abstracts/meps/v318/p1-18/

Feliciano, E. A., Wdowinski, S., & Potts, M. D. (2014). Assessing mangrove above-ground biomass and structure using terrestrial laser scanning: A case study in the Everglades National Park. *Wetlands, 34*(5), 955–968. https://doi.org/10.1007/s13157-014-0558-6

Gijón Mancheño, A., Vuik, V., van Wesenbeeck, B. K., Jonkman, S. N., van Hespen, R., Moll, J. R., Kazi, S., Urrutia, I., & van Ledden, M. (2024). Integrating mangrove growth and failure in coastal flood protection designs. *Scientific Reports, 14*(1), 7951. https://doi.org/10.1038/s41598-024-58705-4

Giri, C., Ochieng, E., Tieszen, L. L., Zhu, Z., Singh, A., Loveland, T., Masek, J., & Duke, N. (2011). Status and distribution of mangrove forests of the world using earth observation satellite data. Global Ecology and Biogeography, 20(1), 154-159. https://doi.org/10.1111/j.1466-8238.2010.00584.x

Hanslow, D. J., Morris, B. D., Foulsham, E., & Kinsela, M. A. (2018). A regional scale approach to assessing current and potential future exposure to tidal inundation in different types of estuaries. *Scientific Reports, 8*(1), 7065. https://doi.org/10.1038/s41598-018-25410-y

Horstman, E. M., Bryan, K. R., & Mullarney, J. C. (2021). Drag variations, tidal asymmetry and tidal range changes in a mangrove creek system. *Earth Surface Processes and Landforms, 46*(9), 1828–1846. https://doi.org/10.1002/esp.5124

Hyyppä, E., Yu, X., Kaartinen, H., Hakala, T., Kukko, A., Vastaranta, M., & Hyyppä, J. (2020). Comparison of backpack, handheld, under-canopy UAV, and above-canopy UAV laser scanning for field reference data collection in boreal forests. *Remote Sensing, 12*(20), 3327.

Kalloe, S. A. (2019). Wave damping potential of woody riparian vegetation: Comparing terrestrial laser scanning with manual measuring techniques Delft University of Technology]. Delft. https://repository.tudelft.nl/islandora/object/uuid%3A6e9c1f7a-4ef9-48ef-bb97-796a9b74fe6b

Kalloe, S. A., Hofland, B., Antolínez, J. A. A., & van Wesenbeeck, B. K. (2022). Quantifying frontal-surface area of woody vegetation: A crucial parameter for wave attenuation [original research]. Frontiers in Marine Science, 9. https://www.frontiersin.org/articles/https://doi.org/10.3389/fmars.2022.820846

Kankare, V., Holopainen, M., Vastaranta, M., Puttonen, E., Yu, X., Hyyppä, J., Vaaja, M., Hyyppä, H., & Alho, P. (2013). Individual tree biomass estimation using terrestrial laser scanning. *ISPRS Journal of Photogrammetry and Remote Sensing, 75*, 64–75. https://doi.org/10.1016/j.isprsjprs.2012.10.003

Kargar, A. R., MacKenzie, R. A., Apwong, M., Hughes, E., & van Aardt, J. (2020). Stem and root assessment in mangrove forests using a low-cost, rapid-scan terrestrial laser scanner. *Wetlands Ecology and Management, 28*(6), 883–900. https://doi.org/10.1007/s11273-020-09753-w

Kauffman, J. B., & Donato, D. C. (2012). Protocols for the measurement, monitoring and reporting of structure, biomass and carbon stocks in mangrove forests. http://www.jstor.org/stable/resrep02318

Kennedy, D. M., McSweeney, S. L., Mariani, M., & Zavadil, E. (2020). The geomorphology and evolution of intermittently open and closed estuaries in large embayments in Victoria. *Australia. Geomorphology, 350*, 106892. https://doi.org/10.1016/j.geomorph.2019.106892

Komiyama, A., Ong, J. E., & Poungparn, S. (2008). Allometry, biomass, and productivity of mangrove forests: A review. *Aquatic Botany, 89*(2), 128–137. https://doi.org/10.1016/j.aquabot.2007.12.006

Komiyama, A., Poungparn, S., & Kato, S. (2005). Common allometric equations for estimating the tree weight of mangroves. *Journal of Tropical Ecology, 21*(4), 471–477. https://doi.org/10.1017/S0266467405002476

Lopez-Arias, F., Maza, M., Calleja, F., Govaere, G., & Lara, J. L. (2024). Integrated drag coefficient formula for estimating the wave attenuation capacity of Rhizophora sp. mangrove forests [Original Research]. Frontiers in Marine Science, 11. https://www.frontiersin.org/journals/marine-science/articles/https://doi.org/10.3389/fmars.2024.1383368

Lovelock, C. E., Bennion, V., Grinham, A., & Cahoon, D. R. (2011). The role of surface and subsurface processes in keeping pace with sea level rise in intertidal wetlands of Moreton Bay, Queensland. *Australia. Ecosystems, 14*(5), 745–757. https://doi.org/10.1007/s10021-011-9443-9

Luetzenburg, G., Kroon, A., Kjeldsen, K. K., Splinter, K. D., & Bjørk, A. A. (2024). High-resolution topographic surveying and change detection with the iPhone LiDAR. *Nature Protocols, 19*(12), 3520–3541. https://doi.org/10.1038/s41596-024-01024-9

Maas, H. G., Bienert, A., Scheller, S., & Keane, E. (2008). Automatic forest inventory parameter determination from terrestrial laser scanner data. *International Journal of Remote Sensing, 29*(5), 1579–1593. https://doi.org/10.1080/01431160701736406

Manly Hydraulics Laboratory. (2024). NSW Water Level Data Collection Program. Retrieved 16/01/2024 from https://mhl.nsw.gov.au/Data-Level

Maza, M., Lara, J. L., & Losada, I. J. (2021). Predicting the evolution of coastal protection service with mangrove forest age. *Coastal Engineering, 168*, 103922. https://doi.org/10.1016/j.coastaleng.2021.103922

Mazda, Y., Wolanski, E., King, B., Sase, A., Ohtsuka, D., & Magi, M. (1997). Drag force due to vegetation in mangrove swamps. *Mangroves and Salt Marshes, 1*(3), 193–199. https://doi.org/10.1023/A:1009949411068

Menéndez, P., Losada, I. J., Torres-Ortega, S., Narayan, S., & Beck, M. W. (2020). The global flood protection benefits of mangroves. *Scientific Reports, 10*(1), 4404. https://doi.org/10.1038/s41598-020-61136-6

Miedema Brown, L., & Anand, M. (2022). Plant functional traits as measures of ecosystem service provision. *Ecosphere, 13*(2), e3930. https://doi.org/10.1002/ecs2.3930

Morris, B., Foulsham, E., Hanslow, D. (2013). Quantifying tidal inundation variations in NSW estuaries NSW Coastal Conference 2013, Port Macquarie, NSW, Australia. https://www.coastalconference.com/2013/papers2013/Brad%20Morris%20Full%20Paper.pdf

Navarro, A., Young, M., Allan, B., Carnell, P., Macreadie, P., & Ierodiaconou, D. (2020). The application of unmanned aerial vehicles (UAVs) to estimate above-ground biomass of mangrove ecosystems. *Remote Sensing of Environment, 242*, 111747. https://doi.org/10.1016/j.rse.2020.111747

Olagoke, A., Proisy, C., Féret, J.-B., Blanchard, E., Fromard, F., Mehlig, U., de Menezes, M. M., dos Santos, V. F., & Berger, U. (2016). Extended biomass allometric equations for large mangrove trees from terrestrial LiDAR data. *Trees, 30*(3), 935–947. https://doi.org/10.1007/s00468-015-1334-9

Owers, C. J., Rogers, K., & Woodroffe, C. D. (2018). Terrestrial laser scanning to quantify above-ground biomass of structurally complex coastal wetland vegetation. *Estuarine, Coastal and Shelf Science, 204*, 164–176. https://doi.org/10.1016/j.ecss.2018.02.027

Pratt, V. (1987). Direct least-squares fitting of algebraic surfaces. *SIGGRAPH Comput. Graph., 21*(4), 145–152. https://doi.org/10.1145/37402.37420

Reid, W., Mooney, HA, Cropper, A, Capistrano, D, Carpenter, SR, Chopra, K, Dasgupta, P, Dietz, T, Duraiappah, AK, Hassan, R, Kasperson, R, Leemans, R, May, RM, McMichael, AJ, Pingali, P, Samper, C, Scholes, R, Watson, RT, Zakri, AH, Shidong, Z, Ash, NJ, Bennett, E, Kumar, P, Lee, MJ, Raudsepp-Hearne, C, Simons, H, Thonell, J & Zurek, MB. (2005). Ecosystems and human well-being - Synthesis: A report of the millennium ecosystem assessment. I. Press. https://www.millenniumassessment.org/documents/document.353.aspx.pdf

RIEGL. (2024). RIEGL VZ-600i Data Sheet. http://www.riegl.com/uploads/tx_pxpriegldownloads/RIEGL_VZ-600i_Datasheet_2024-11-13.pdf

Ryding, J., Williams, E., Smith, M. J., & Eichhorn, M. P. (2015). Assessing handheld mobile laser scanners for forest surveys. *Remote Sensing, 7*(1), 1095–1111.

Salmo, S. G., Lovelock, C., & Duke, N. C. (2013). Vegetation and soil characteristics as indicators of restoration trajectories in restored mangroves. *Hydrobiologia, 720*(1), 1–18. https://doi.org/10.1007/s10750-013-1617-3

Simard, M., Fatoyinbo, L., Thomas, N. M., Stovall, A. E., Parra, A., Barenblitt, A., Bunting, P., & Hajnsek, I. (2025). A new global mangrove height map with a 12 meter spatial resolution. *Scientific Data, 12*(1), 15. https://doi.org/10.1038/s41597-024-04213-z

Sippo, J. Z., Sanders, C. J., Santos, I. R., Jeffrey, L. C., Call, M., Harada, Y., Maguire, K., Brown, D., Conrad, S. R., & Maher, D. T. (2020). Coastal carbon cycle changes following mangrove loss. *Limnology and Oceanography, 65*(11), 2642–2656. https://doi.org/10.1002/lno.11476

Suzuki, T., Zijlema, M., Burger, B., Meijer, M. C., & Narayan, S. (2012). Wave dissipation by vegetation with layer schematization in SWAN. *Coastal Engineering, 59*(1), 64–71. https://doi.org/10.1016/j.coastaleng.2011.07.006

Tukey, J. W. (1949). Comparing individual means in the analysis of variance. *Biometrics, 5*(2), 99–114. https://doi.org/10.2307/3001913

Twomey, A. J., & Lovelock, C. E. (2025). Variation in mangrove geometric traits among genera and climate zones. *Estuaries and Coasts, 48*(2), 55. https://doi.org/10.1007/s12237-025-01487-3

van Wesenbeeck, B. K., Wolters, G., Antolínez, J. A. A., Kalloe, S. A., Hofland, B., de Boer, W. P., Çete, C., & Bouma, T. J. (2022). Wave attenuation through forests under extreme conditions. *Scientific Reports, 12*(1), 1884. https://doi.org/10.1038/s41598-022-05753-3

van Zelst, V. T. M., Dijkstra, J. T., van Wesenbeeck, B. K., Eilander, D., Morris, E. P., Winsemius, H. C., Ward, P. J., & de Vries, M. B. (2021). Cutting the costs of coastal protection by integrating vegetation in flood defences. *Nature Communications, 12*(1), 6533. https://doi.org/10.1038/s41467-021-26887-4

Warfield, A. D., & Leon, J. X. (2019). Estimating mangrove forest volume using terrestrial laser scanning and UAV-derived structure-from-motion. *Drones, 3*(2), 32.

Wilkes, P., Disney, M., Armston, J., Bartholomeus, H., Bentley, L., Brede, B., Burt, A., Calders, K., Chavana-Bryant, C., Clewley, D., Duncanson, L., Forbes, B., Krisanski, S., Malhi, Y., Moffat, D., Origo, N., Shenkin, A., & Yang, W. (2023). TLS2trees: A scalable tree segmentation pipeline for TLS data. *Methods in Ecology and Evolution, 14*(12), 3083–3099. https://doi.org/10.1111/2041-210X.14233

Wu, C., Yuan, Y., Tang, Y., & Tian, B. (2022). Application of terrestrial laser scanning (TLS) in the architecture, engineering and construction (AEC) industry. *Sensors, 22*(1), 265.

Zhang, K., Liu, H., Li, Y., Xu, H., Shen, J., Rhome, J., & Smith, T. J. (2012). The role of mangroves in attenuating storm surges. *Estuarine, Coastal and Shelf Science, 102–103*, 11–23. https://doi.org/10.1016/j.ecss.2012.02.021

Zhang, R., Chen, Y., Lei, J., Zhou, X., Yao, P., & Stive, M. J. F. (2023). Experimental investigation of wave attenuation by mangrove forests with submerged canopies. *Coastal Engineering, 186*, 104403. https://doi.org/10.1016/j.coastaleng.2023.104403

Zhao, Y., Jungho, I., Zhen, Z., & Zhao, Y. (2023). Towards accurate individual tree parameters estimation in dense forest: Optimized coarse-to-fine algorithms for registering UAV and terrestrial LiDAR data. *GIScience & Remote Sensing, 60*(1), 2197281. https://doi.org/10.1080/15481603.2023.2197281